

Strain-Driven Approach to Quantum Criticality in $A\text{Fe}_2\text{As}_2$ with $A = \text{K}, \text{Rb}$, and Cs

Felix Eilers,¹ Kai Grube,¹ Diego A. Zocco,¹ Thomas Wolf,¹ Michael Merz,¹ Peter Schweiss,¹ Rolf Heid,¹ Robert Eder,¹ Rong Yu,² Jian-Xin Zhu,³ Qimiao Si,⁴ Takasada Shibauchi,^{5,6} and Hilbert v. Löhneysen^{1,7}

¹Institut für Festkörerphysik, Karlsruher Institut für Technologie, 76021 Karlsruhe, Germany

²Department of Physics, Renmin University of China, Beijing 100872, China

³Theoretical Division, Los Alamos National Laboratory, Los Alamos, New Mexico 87545, USA

⁴Department of Physics and Astronomy, Rice University, Houston, Texas 77005, USA

⁵Department of Advanced Materials Science, University of Tokyo, Kashiwa, Chiba 277-8561, Japan

⁶Department of Physics, Kyoto University, Sakyo-ku, Kyoto 606-8502, Japan

⁷Physikalisches Institut, Karlsruher Institut für Technologie, 76049 Karlsruhe, Germany

(Received 7 October 2015; revised manuscript received 8 April 2016; published 8 June 2016)

The iron-based superconductors $A\text{Fe}_2\text{As}_2$ with $A = \text{K}, \text{Rb}, \text{Cs}$ exhibit large Sommerfeld coefficients approaching those of heavy-fermion systems. We have investigated the magnetostriction and thermal expansion of this series to shed light on this unusual behavior. Quantum oscillations of the magnetostriction allow identifying the band-specific quasiparticle masses which by far exceed the band-structure derived masses. The divergence of the Grüneisen ratio derived from thermal expansion indicates that with increasing volume along the series a quantum critical point is approached. The critical fluctuations responsible for the enhancement of the quasiparticle masses appear to weaken the superconducting state.

DOI: 10.1103/PhysRevLett.116.237003

Unconventional superconductivity (SC) often emerges in the proximity of continuous, zero-temperature phase transitions, so-called quantum critical points (QCPs). In particular, the onset of magnetic order is generally believed to drive SC by magnetic quantum criticality. Examples encompass the cuprates, organic metals, heavy-fermion systems, and the recently discovered iron-based superconductors. A particularly illustrative example is given by $\text{BaFe}_2(\text{As}_{1-x}\text{P}_x)_2$. Here, the application of chemical pressure, by replacing As with isovalent, smaller P ions, suppresses antiferromagnetic (AFM) order resulting in an extended superconducting dome with a maximum transition temperature $T_c \approx 30$ K at the critical concentration $x_c = 0.3$ [1]. The QCP at x_c shielded by SC was anticipated theoretically [2] and observed through strongly enhanced quasiparticle masses and deviations from Fermi-liquid (FL) behavior. In this Letter, we show that the isostructural superconductor KFe_2As_2 can likewise be pushed towards a QCP by substituting isovalent, but larger Rb and Cs for K. In these compounds, in contrast to the examples listed above and despite general consensus, quantum criticality fails to boost SC.

The alkali metal series $A\text{Fe}_2\text{As}_2$ (A122) with $A = \text{K}, \text{Rb}$, and Cs , represent one of the rare examples of stoichiometric iron-arsenide superconductors. According to local-density approximation (LDA) calculations their low- T_c values of less than 3.5 K cannot be explained by electron-phonon coupling [3]. Angle-resolved photoemission spectroscopy and thermal-conductivity measurements suggest an unconventional pairing mechanism [4–7]. Recent specific-heat measurements reveal huge Sommerfeld coefficients γ which exceed those of $\text{BaFe}_2(\text{As}_{1-x}\text{P}_x)_2$ in apparent

contradiction to the low- T_c values [7–9]. In order to elucidate the highly correlated normal state and its relationship to SC, we investigated the quantum oscillations observable in the magnetostriction of the A122 series.

Single-crystalline samples were grown from an arsenic-rich flux, yielding T_c values of 3.40(5), 2.53(3), and 2.27(4) K for $A = \text{K}, \text{Rb}$, and Cs , respectively [10]. The low impurity concentration of the crystals allows observing quantum oscillations of the sample length as a function of the applied magnetic field B ranging between the upper critical field B_{c2} and the maximum field of 14 T (insets of Fig. 1). The mean free paths determined from the field dependence of these oscillations confirm that the decreasing T_c values in the A122 series do not arise from varying sample quality [10]. To extract the fundamental frequencies, we performed a Fourier transformation of the oscillatory part of the measured magnetostriction coefficient $\lambda_i \equiv L_i^{-1} \partial L_i / \partial B$, where L_i is the sample length along the tetragonal $i = a$ and c directions.

The spectra of the three A122 compounds taken at $T = 50$ mK for $B \parallel a$ and c , are plotted as amplitude against frequency F in Fig. 1. The data of K122 are taken from Refs. [28–30]. The difference between the λ_a and λ_c spectra reflects the anisotropic uniaxial pressure dependences of the Fermi-surface (FS) cross sections [31]. The observed sharp peaks mark the fundamental and higher harmonic cyclotron frequencies corresponding to the extremal orbits of the FS, which have been assigned to specific bands by comparing the spectra of Rb122 and Cs122 to those of K122 and to our LDA calculations. For $A = \text{Rb}$ and Cs , all FS sheets apart from the β band could be identified. As the isovalent substitution of A keeps the total hole count

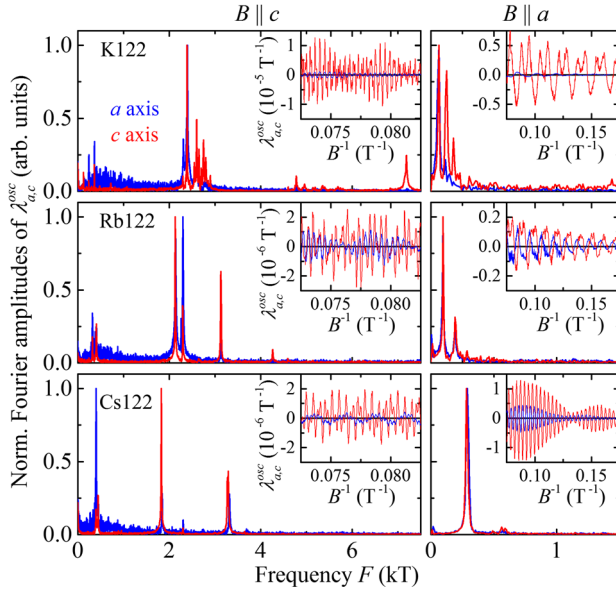


FIG. 1. Normalized Fourier spectra of the oscillatory part of the magnetostriction coefficient λ_i^{osc} (insets) along the $i = a$ (blue) and c axis (red line) of A122, $A = \text{K}, \text{Rb}$, and Cs , at $T = 50$ mK for $B \parallel c$ and a .

constant we can estimate the contribution of the β sheet by subtracting the cross sections of all other bands from the FS volume of K122. In Fig. 2(a) the obtained extremal cross-sectional areas, expressed as fractions of the volume of the first Brillouin zone, are plotted against the radius of the alkali-metal ion R_A .

In line with our LDA calculations, the data show no change of the FS topology with increasing R_A . The

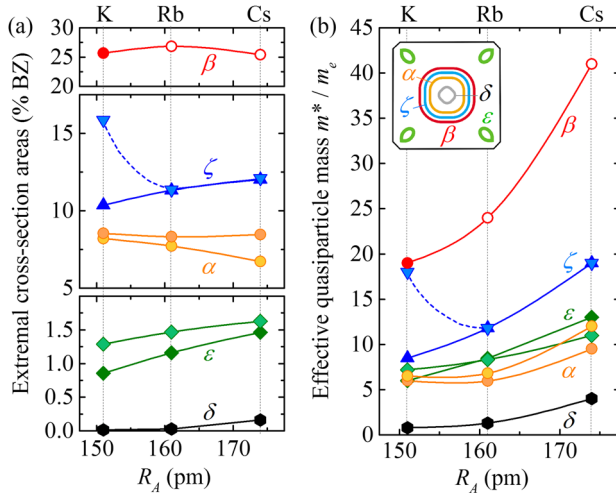


FIG. 2. (a) Extremal cross-sectional areas of the Fermi surfaces of $(\text{K},\text{Rb},\text{Cs})122$, expressed as fractions of the first Brillouin-zone volumes. (b) Effective quasiparticle masses m^* , plotted against the ionic radius of the alkaline atom R_A [28–30]. The values presented by open symbols were obtained by assuming a constant total hole count and using the Sommerfeld coefficients [7–9]. Lines are guides to the eye.

two-dimensionality of the FeAs-layered structure is reflected by three tubes in the Brillouin-zone center [α , ζ , and β , see inset of Fig. 2(b)] and one tube at each corner (ϵ). Marginal three-dimensional features were inferred from closely spaced peaks in the Fourier spectra, indicating a gentle warping of the FS tubes, and from a single fundamental frequency for $B \parallel a$, attributed to a tiny pocket at the top center. So far, this pocket has been seen only in magnetostriction measurements [30].

The decay of the oscillations with increasing T [10] is used to determine the effective quasiparticle masses m_j^* of each FS sheet j . Since in quasi-two-dimensional systems the Sommerfeld coefficient is given by $\gamma \approx (\pi k_B^2 N_A a^2 / 3\hbar^2) \sum_j m_j^*$ (N_A is Avogadro's number), the mass of the β tube can be determined by subtracting the contributions of all other bands from the published γ values. For the warped FS tubes we simply used the average value of the effective masses assuming a sinusoidal warping. The obtained large m_β^* values alone cannot account for the absence of β -band oscillations in our measurements. The β -band FS cross section does, however, hardly depend on R_A , suggesting small uniaxial pressure effects and, therefore, further reduced $\lambda_i^{\text{osc}(\beta)}$ amplitudes. Figure 2(b) summarizes the resulting quasiparticle masses as a function of R_A . Not only m_β^* , but also all effective masses exhibit significant increases with R_A , with a factor of $m_j^*(\text{Cs})/m_j^*(\text{K}) \approx 2$, which interestingly is similar to that of $\gamma(\text{Cs})/\gamma(\text{K})$. LDA calculations, on the other hand, predict band masses an order of magnitude smaller, with a comparatively slight increase towards Cs122. This difference reinforces the assumption that the huge low-temperature specific heat arises from strong electronic correlations (see below).

The negative chemical pressure exerted upon replacing K by the larger Rb or Cs ions mainly expands the c axis by pushing the FeAs layers further apart from each other. To elucidate the difference between chemical and external, hydrostatic pressure, we performed thermal-expansion measurements. In a FL, the uniaxial pressure dependence of the Sommerfeld coefficient is related to the linear thermal-expansion coefficient α_i by $\partial\gamma/\partial p_i = -(V/T)\alpha_i$, where V is the molar volume and p_i uniaxial pressure in the $i = a, c$ direction. The hydrostatic pressure dependence is given by $\partial\gamma/\partial p = 2\partial\gamma/\partial p_a + \partial\gamma/\partial p_c$. Between T_c and 4 K, all three compounds show FL behavior, i.e., constant α_i/T values, similarly to the published C/T data. With increasing R_A and, consequently, growing unit-cell volume, the pressure dependence decreases from $\partial\gamma/\partial p = -20.3$ mJ/mol K² GPa (K) [32] to -36.6 mJ/mol K² GPa (Rb) and -77.7 mJ/mol K² GPa (Cs) suggesting a nonlinear V dependence of γ . In order to compare with the chemical pressure effect, we convert the hydrostatic pressure dependences from our thermal expansion measurements to volume derivatives $\partial\gamma/\partial V = -V^{-1} B_T \partial\gamma/\partial p$, and estimate $\gamma_p(V)$ by integrating over the obtained $\partial\gamma(V)/\partial V$ values. Here, $B_T = -V\partial p/\partial V$ is the bulk

modulus. The integration constant is provided by the published γ values of K122. In a first step we take V to be the unit-cell volume V_{UC} using $B_T(V_{UC}) \approx 40$ GPa of K122 [33]. The calculated $\gamma_p(V_{UC})$ curves are displayed in Fig. 3(a) together with the Sommerfeld coefficients $\gamma(V_{UC})$ at ambient pressure [7–9,34]. Obviously, $\gamma_p(V_{UC})$ strongly overestimates the chemical pressure effect $\gamma(V_{UC})$. In this simple estimate we have neglected that chemical and hydrostatic pressures affect the crystal structure in different

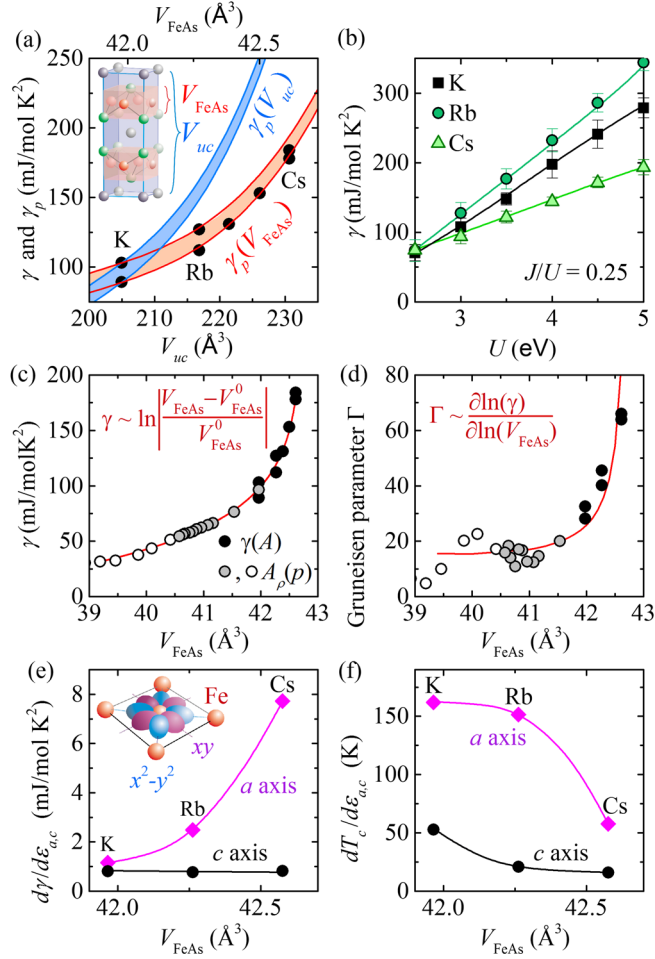


FIG. 3. (a) Comparison between chemical (black dots) and hydrostatic pressure dependences of the Sommerfeld coefficient γ as a function of the unit-cell volume V_{UC} and that of a single FeAs layer V_{FeAs} . The hydrostatic pressure dependences are extracted from the volume thermal expansion α_V for $V = V_{UC}$ (blue lines) and V_{FeAs} (red lines). (b) The calculated γ as a function of U in a multiorbital Hubbard model for A122 ($A = K, Rb, Cs$) (see text). (c) Evolution of the measured γ with increasing V_{FeAs} . Gray [35] and open dots [36] are estimated from high-pressure resistivity measurements. The red line is a fit to the data points. (d) The Grüneisen parameter Γ , calculated from γ, A_ρ , and α_V . The red line is determined with the fit shown in (d) under the assumption of a Fermi liquid. (e) Strain dependences of γ and (f) the superconducting transition temperature T_c . Lines are guides to the eyes. The inset in (e) shows the Fe plane with the $3d_{xy}$ and $3d_{x^2-y^2}$ orbitals.

ways: while the latter leads to a reduction or increase of *all* bond lengths, the alkali-metal substitution changes c and FeAs-layer thickness h_{FeAs} with opposite trends: it increases c and decreases h_{FeAs} [10]. Therefore, in a second step, we perform the comparison on the basis of the FeAs-cell volume $V_{FeAs} = a^2 h_{FeAs}$. The related bulk modulus of $B_T(V_{FeAs}) \approx 145$ GPa was inferred from the high-pressure data of K122 [33]. The estimated $\gamma_p(V_{FeAs})$ curves are likewise shown in Fig. 3(a). Taking V_{FeAs} as the decisive p -dependent volume, hydrostatic and chemical pressure dependences coincide with each other. This agreement suggests that the enhanced correlations originate from a change of the direct Fe environment due to a reduced hybridization of the Fe $3d$ states with nearest-neighbor Fe or As orbitals.

The role of the FeAs-cell volume was pointed out in recent publications [37–41], and provides the basis to study the evolution of electronic correlations in a wider phase space. We extended the pressure dependence of γ to smaller V_{FeAs} values by resorting to resistivity measurements of K122 under hydrostatic pressure [35,36]. Since the FL state of K122 follows the Kadowaki-Woods (KW) relation [42] we relate γ to the scattering cross section A_ρ of the low-temperature resistivity $\rho = \rho_0 + A_\rho T^2$ by using a proportionality factor of $A_\rho/\gamma^2 \approx 2 \times 10^{-6} \mu\Omega\text{cm(K mol/mJ)}^2$ so that the ambient pressure measurements are reproduced [42]. The extended $\gamma(V_{FeAs})$ data displayed in Fig. 3(c) exhibit the characteristic sudden increase of a system that is tuned towards a QCP. The best fit to this mass divergence is given by a logarithmic volume dependence $\gamma \propto \ln(|V_{FeAs} - V_{FeAs}^0|/V_{FeAs}^0)$, with $V_{FeAs}^0 = 42.72 \text{ \AA}^3$, as proposed for a two-dimensional FL close to a Mott transition and found for $\text{BaFe}_2(\text{As}_{1-x}\text{P}_x)_2$ [43].

QCPs are characterized by a vanishing characteristic energy scale E^* , leading to a divergence of the Grüneisen parameter $\Gamma \approx -d\ln(E^*)/\ln(V)$ for a pressure-induced QCP. We calculated $\Gamma = V_{FeAs} B_T(V_{FeAs}) \alpha_V / \gamma$ from our thermal expansion data $\alpha_V = 2\alpha_a + \alpha_c$. For the high-pressure resistivity measurements we use $\Gamma = d\ln(\gamma)/d\ln(V_{FeAs}) = (1/2)d\ln(A_\rho)/d\ln(V_{FeAs})$ by virtue of the KW relation. The volume dependence of Γ , shown in Fig. 3(d), clearly exhibits a pronounced divergence. This provides [44,45] clear evidence that with increasing R_A a QCP is approached and Cs122 is in its close proximity. Recent resistivity measurements of Cs122 do report indications of non-FL behavior [6].

To specify the hybridized orbitals responsible for the critical mass enhancement, we determine the uniaxial pressure dependences $\partial\gamma/\partial p_i$ for $i = a, c$ from α_i . Furthermore, we approximate the elastic constants c_{ij} of the A122 compounds by density-functional theory calculations [10] to obtain an estimate of the strain dependences $d\gamma/d\epsilon_i = \sum c_{ij} d\gamma/dp_j$. The $d\gamma/d\epsilon_i$ values show that with increasing V_{FeAs} , mainly a -axis changes account for the mass enhancement [Fig. 3(e)]. In particular, the divergence

can be observed only in $d\gamma/d\epsilon_a$. This allows identifying the orbitals involved, as in the FeAs-cell volume, only the Fe $3d_{xy}$ or $3d_{x^2-y^2}$ orbitals are confined to the ab plane [inset of Fig. 3(e)] and are, therefore, affected by a - or b -axis changes. Since the band-specific masses shown in Fig. 2 reveal the heaviest masses for the β bands with dominating d_{xy} character, we conclude that the critical mass enhancement can be attributed to the hybridization of the in-plane d_{xy} orbitals.

If, as suggested, in the traditional QCP scenario SC is supported by critical fluctuations arising close to a QCP, the strain dependence $\partial T_c/\partial\epsilon_i$ should follow that of $\partial\gamma/\partial\epsilon_i$. To check this scenario, we determine the uniaxial pressure dependences of T_c by using the Ehrenfest relations with the discontinuities of α_i and C at T_c , and convert them to $\partial T_c/\partial\epsilon_i$. Similarly to $\partial\gamma/\partial\epsilon_c$, changes of the c axis hardly affect T_c [Fig. 3(f)]. Contrary to the expectation of the above scenario, however, $\partial T_c/\partial\epsilon_a$ shows a behavior opposite to that of $\partial\gamma/\partial\epsilon_a$, and decreases with increasing V_{FeAs} . This apparent dichotomy suggests that the d_{xy} states driving the mass enhancement tend to simultaneously weaken SC. Because of the minor FS variations with R_A , a change of the electronic structure and nesting conditions can hardly account for the T_c reduction.

The specific role of the Fe $3d$ levels for the electronic correlations in Fe-based superconductors reflects the Coulomb (Hubbard and Hund) interactions as well as the small crystal-electric-field splittings [39,40,46–49]. To better understand the observed mass enhancement, we study [10] the electron correlation effects in a multi-orbital Hubbard model for A122 using a $U(1)$ slave-spin mean-field theory [50]. The details of the model and the method can be found in the Supplemental Material [10]. The A122 system corresponds to a $3d$ -electron filling of $N = 5.5$ per Fe atom. For this filling, we identify a strongly correlated regime for a range of realistic values for U and J (Fig. S4 of Ref. [10]). In this regime, the quasiparticle spectral weights in all five Fe $3d$ orbitals are substantially reduced, and a strong orbital dependence arises. As shown in Fig. S5, the quasiparticle spectral weight of the d_{xy} orbital is most strongly reduced, correspondingly, its mass enhancement is the largest. We further calculate the Sommerfeld coefficient γ . As shown in Fig. 3(b), the calculated γ values have a magnitude similar to the experimental values. However, for fixed values of the interactions, γ does not show a strong increase across the K through Rb to Cs series. We attribute this missing contribution to an additional component of γ arising from the proximity to quantum criticality.

The emerging picture is summarized in Fig. 4 which depicts γ in the (N, V_{FeAs}) plane. The γ values of the series $\text{Ba}_x\text{K}_{1-x}\text{Fe}_2\text{As}_2$ [51], where $N = 6 - x/2$ varies from $N = 5.5$ to 6, contrast with those of $\text{BaFe}_2(\text{As}_{1-x}\text{P}_x)_2$, where $N = 6$ and V_{FeAs} changes significantly [1,52]. Both series exhibit a maximum γ_{max} close to the onset of AFM

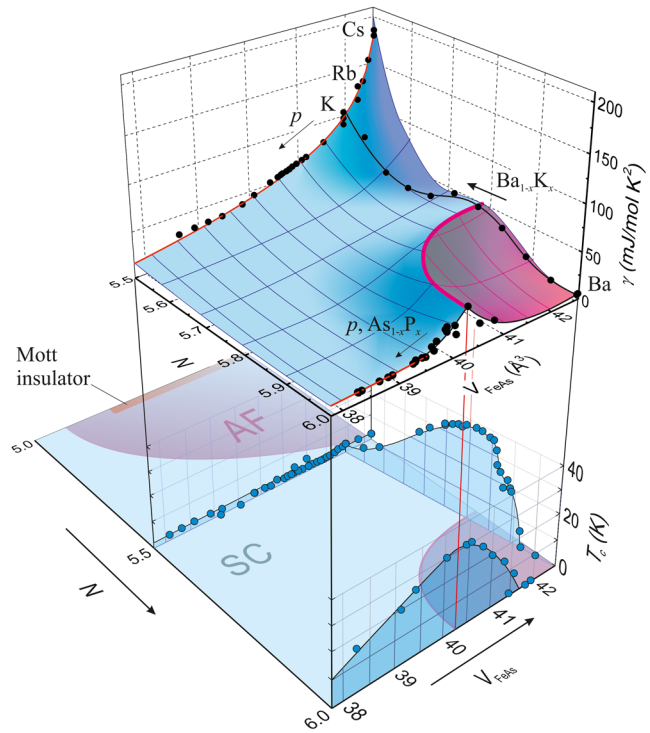


FIG. 4. Evolution of γ as a function of V_{FeAs} and hole doping expressed as filling N of the Fe $3d$ states. In addition to the high-pressure data of KFe_2As_2 [33,35,36,53], measurements of $\text{Ba}_{1-x}\text{K}_x\text{Fe}_2\text{As}_2$ [51,54] and $\text{BaFe}_2(\text{As}_{1-x}\text{P}_x)_2$ [1,52,55,56] have been included. The γ values of $\text{BaFe}_2(\text{As}_{1-x}\text{P}_x)_2$ were estimated following Ref. [52]. The base plane shows a tentative phase diagram of a five-orbital Hubbard model with combined (U, J) interactions leading to a Mott-insulating state at $N = 5$ [46].

order suggesting an underlying QCP. However, the highest γ value is found for the A122 compounds where T_c values are one order of magnitude smaller than those of $\text{Ba}_x\text{K}_{1-x}\text{Fe}_2\text{As}_2$ and $\text{BaFe}_2(\text{As}_{1-x}\text{P}_x)_2$. Figure 4 strongly suggests that the QCP suggested by our measurements would be most naturally associated with an AFM order related to the $N = 5$ Mott-insulating phase [46].

The combined effect of Hund's rule coupling and Coulomb exchange interaction is considerably intensified by reducing the bandwidth. This is exemplified by $\text{BaFe}_2(\text{As}_{1-x}\text{P}_x)_2$ and A122. While in $\text{BaFe}_2(\text{As}_{1-x}\text{P}_x)_2$ the hybridization changes due to longer Fe–As bonds, in the A122 series only the Fe–Fe distances are widened [10,55]. Remarkably, the largest γ values are found for A122 with a divergent trend towards $A = \text{Cs}$. These high values do not find any correspondence in the superconducting properties. In fact, it seems that here strong correlations weaken SC which might occur on rather general grounds [57,58].

We speculate that the A122 series might be a candidate for the special situation where a QCP exactly coincides with the onset of SC. This could provide a new insight into the physics of iron pnictides close to the $N = 5$ limit which

should be tested by investigating Cs122 films under tensile biaxial strain.

We thank Y. Mizukami, H. Ikeda, T. Terashima, P. Adelmann, F. Hardy, A. E. Böhmer, C. Meingast, J. Schmalian, L. de' Medici, M. Capone, M. Grosche, and J. Wosnitza for valuable discussions. This work has been supported by Deutsche Forschungsgemeinschaft in the frame of FOR960 (Quantum Phase Transitions) and the Japan-Germany Research Cooperative Program, KAKENHI from JSPS and Project No. 56393598 from DAAD. The work was in part supported by the U.S. DOE at LANL under Contract No. DE-AC52-06NA25396 and the DOE Office of Basic Energy Sciences (J.-X. Z.), by the National Science Foundation of China Grant No. 11374361, the Fundamental Research Funds for the Central Universities and the Research Research Funds of Renmin University of China (R. Y.), and by the NSF and the Robert A. Welch Foundation Grant No. C-1411 (Q. S.). Q. S. also acknowledges the support of the Alexander von Humboldt Foundation through a Humboldt Research Award and the hospitality of the Karlsruhe Institute of Technology. H. v. L. and Q. S. enjoyed the hospitality of the Aspen Center for Physics when finalizing the manuscript (supported by NSF Grant No. PHY-1066293).

- [1] T. Shibauchi, A. Carrington, and Y. Matsuda, *Annu. Rev. Condens. Matter Phys.* **5**, 113 (2014).
- [2] J. Dai, Q. Si, J.-X. Zhu, and E. Abrahams, *Proc. Natl. Acad. Sci. U.S.A.* **106**, 4118 (2009).
- [3] Y. G. Naidyuk, O. E. Kvitnitskaya, N. V. Gamayunova, L. Boeri, S. Aswartham, S. Wurmehl, B. Büchner, D. V. Efremov, G. Fuchs, and S.-L. Drechsler, *Phys. Rev. B* **90**, 094505 (2014).
- [4] K. Okazaki, Y. Ota, Y. Kotani, W. Malaeb, Y. Ishida, T. Shimojima, T. Kiss, S. Watanabe, C.-T. Chen, K. Kihou, C. H. Lee, A. Iyo, H. Eisaki, T. Saito, H. Fukazawa, Y. Kohori, K. Hashimoto, T. Shibauchi, Y. Matsuda, H. Ikeda, H. Miyahara, R. Arita, A. Chainani, and S. Shin, *Science* **337**, 1314 (2012).
- [5] J.-P. Reid, M. A. Tanatar, A. Juneau-Fecteau, R. T. Gordon, S. R. de Cotret, N. Doiron-Leyraud, T. Saito, H. Fukazawa, Y. Kohori, K. Kihou, C. H. Lee, A. Iyo, H. Eisaki, R. Prozorov, and L. Taillefer, *Phys. Rev. Lett.* **109**, 087001 (2012).
- [6] X. C. Hong, X. L. Li, B. Y. Pan, L. P. He, A. F. Wang, X. G. Luo, X. H. Chen, and S. Y. Li, *Phys. Rev. B* **87**, 144502 (2013).
- [7] Z. Zhang, A. F. Wang, X. C. Hong, J. Zhang, B. Y. Pan, J. Pan, Y. Xu, X. G. Luo, X. H. Chen, and S. Y. Li, *Phys. Rev. B* **91**, 024502 (2015).
- [8] F. Hardy, A. E. Böhmer, D. Aoki, P. Burger, T. Wolf, P. Schweiss, R. Heid, P. Adelmann, Y. X. Yao, G. Kotliar, J. Schmalian, and C. Meingast, *Phys. Rev. Lett.* **111**, 027002 (2013).

- [9] A. F. Wang, B. Y. Pan, X. G. Luo, F. Chen, Y. J. Yan, J. J. Ying, G. J. Ye, P. Cheng, X. C. Hong, S. Y. Li, and X. H. Chen, *Phys. Rev. B* **87**, 214509 (2013).
- [10] See Supplemental Material at <http://link.aps.org/supplemental/10.1103/PhysRevLett.116.237003>, which includes Refs. [11–27], for a description of the theoretical methods and experimental details.
- [11] E. Fawcett *et al.*, *Electrons at the Fermi Surface*, edited by M. Springford (Cambridge University Press, Cambridge, 1980).
- [12] B. Meyer, C. Elsässer, M. Lechermann, and F. Fähnle, *FORTRAN90: A Program for Mixed-Basis Pseudopotential Calculations for Crystals* (MPI für Metallforschung, Stuttgart, unpublished).
- [13] R. Heid and K.-P. Bohnen, *Phys. Rev. B* **60**, R3709 (1999).
- [14] M. Born and K. Huang, *Dynamical Theory of Crystal Lattices* (Oxford University Press, Oxford, 1954).
- [15] R. Mittal, L. Pintschovius, D. Lamago, R. Heid, K.-P. Bohnen, D. Reznik, S. L. Chaplot, Y. Su, N. Kumar, S. K. Dhar, A. Thamizhavel, and T. Brueckel, *Phys. Rev. Lett.* **102**, 217001 (2009).
- [16] D. Reznik, K. Lokshin, D. C. Mitchell, D. Parshall, W. Dmowski, D. Lamago, R. Heid, K.-P. Bohnen, A. S. Sefat, M. A. McGuire, B. C. Sales, D. G. Mandrus, A. Subedi, D. J. Singh, A. Alatas, M. H. Upton, A. H. Said, A. Cunsolo, Y. Shvyd'ko, and T. Egami, *Phys. Rev. B* **80**, 214534 (2009).
- [17] C. Castellani, C. R. Natoli, and J. Ranninger, *Phys. Rev. B* **18**, 4945 (1978).
- [18] R. Yu and Q. Si, *Phys. Rev. Lett.* **110**, 146402 (2013).
- [19] T. Yoshida, S.-i. Ideta, I. Nishi, A. Fujimori, M. Yi, R. Moore, S.-K. Mo, D. Lu, Z.-X. Shen, Z. Hussain, K. Kihou, C. H. Lee, A. Iyo, H. Eisaki, and H. Harima, *Front. Phys.* **2**, 17 (2014).
- [20] S. Kong, D. Y. Liu, S. T. Cui, S. L. Ju, A. F. Wang, X. G. Luo, L. J. Zou, X. H. Chen, G. B. Zhang, and Z. Sun, *Phys. Rev. B* **92**, 184512 (2015).
- [21] P. Blaha, K. Schwarz, G. Madsen, D. Kvasnicka, and J. Luitz, *WIEN2k: An Augmented Plane Wave+Local Orbitals Program for Calculating Crystal Properties* (Karlheinz Schwarz, Techn. Universität Wien, Austria, Wien, 2001).
- [22] S. Graser, A. F. Kemper, T. A. Maier, H.-P. Cheng, P. J. Hirschfeld, and D. J. Scalapino, *Phys. Rev. B* **81**, 214503 (2010).
- [23] N. Marzari and D. Vanderbilt, *Phys. Rev. B* **56**, 12847 (1997).
- [24] I. Souza, N. Marzari, and D. Vanderbilt, *Phys. Rev. B* **65**, 035109 (2001).
- [25] S. Graser, T. A. Maier, P. J. Hirschfeld, and D. J. Scalapino, *New J. Phys.* **11**, 025016 (2009).
- [26] J. Kuneš, R. Arita, P. Wissgott, A. Toschi, H. Ikeda, and K. Held, *Comput. Phys. Commun.* **181**, 1888 (2010).
- [27] A. A. Mostofi, J. R. Yates, Y.-S. Lee, I. Souza, D. Vanderbilt, N. Marzari, A. A. Mostofi, J. R. Yates, Y.-S. Lee, I. Souza, D. Vanderbilt, and N. Marzari, *Comput. Phys. Commun.* **178**, 685 (2008).
- [28] T. Terashima, N. Kurita, M. Kimata, M. Tomita, S. Tsuchiya, M. Imai, A. Sato, K. Kihou, C.-H. Lee, H. Kito, H. Eisaki, A. Iyo, T. Saito, H. Fukazawa, Y. Kohori, H. Harima, and S. Uji, *Phys. Rev. B* **87**, 224512 (2013).
- [29] D. A. Zocco, K. Grube, F. Eilers, T. Wolf, and H. v. Löhneysen, *Phys. Rev. Lett.* **111**, 057007 (2013).

- [30] D. A. Zocco, K. Grube, F. Eilers, T. Wolf, and H. v. Löhneysen, *J. Phys. Soc. Jpn. Conf. Proc.* **3**, 015007 (2014).
- [31] D. Shoenberg, *Magnetic Oscillations in Metals* (Cambridge University Press, Cambridge, 1984).
- [32] P. Burger, F. Hardy, D. Aoki, A. E. Böhmer, R. Eder, R. Heid, T. Wolf, P. Schweiss, R. Fromknecht, M. J. Jackson, C. Paulsen, and C. Meingast, *Phys. Rev. B* **88**, 014517 (2013).
- [33] F. F. Tafti, J. P. Clancy, M. Lapointe-Major, C. Collignon, S. Faucher, J. A. Sears, A. Juneau-Fecteau, N. Doiron-Leyraud, A. F. Wang, X.-G. Luo, X. H. Chen, S. Desgreniers, Y.-J. Kim, and L. Taillefer, *Phys. Rev. B* **89**, 134502 (2014).
- [34] J. Kanter, Z. Bukowski, J. Karpinski, and B. Batlogg, in *Annual Report of the Laboratory for Solid State Physics* (ETH Zürich, Department of Physics, Zürich, 2010).
- [35] V. Taufour, N. Foroozani, M. A. Tanatar, J. Lim, U. Kaluarachchi, S. K. Kim, Y. Liu, T. A. Lograsso, V. G. Kogan, R. Prozorov, S. L. Bud'ko, J. S. Schilling, and P. C. Canfield, *Phys. Rev. B* **89**, 220509 (2014).
- [36] L.-Y. T. Jian-Jun Ying, V. V. Struzhkin, H.-K. Mao, A. G. Gavriliuk, A.-F. Wang, X.-H. Chen, and X.-J. Chen, [arXiv:1501.00330](https://arxiv.org/abs/1501.00330).
- [37] S. Drotziger, P. Schweiss, K. Grube, T. Wolf, P. Adelmann, C. Meingast, and H. v. Löhneysen, *J. Phys. Soc. Jpn.* **79**, 124705 (2010).
- [38] E. Granado, L. Mendonça Ferreira, F. Garcia, G. d. M. Azevedo, G. Fabbris, E. M. Bittar, C. Adriano, T. M. Garitezi, P. F. S. Rosa, L. F. Bufaiçal, M. A. Avila, H. Terashita, and P. G. Pagliuso, *Phys. Rev. B* **83**, 184508 (2011).
- [39] Z. P. Yin, K. Haule, and G. Kotliar, *Nat. Mater.* **10**, 932 (2011).
- [40] T. T. Ong and P. Coleman, *Phys. Rev. Lett.* **108**, 107201 (2012).
- [41] P. F. S. Rosa, T. M. Adriano, C. Garitezi, T. Grant, Z. Fisk, R. R. Urbano, and P. G. Pagliuso, *Sci. Rep.* **4**, 6543 (2014).
- [42] K. Hashimoto, A. Serafin, S. Tonegawa, R. Katsumata, R. Okazaki, T. Saito, H. Fukazawa, Y. Kohori, K. Kihou, C. H. Lee, A. Iyo, H. Eisaki, H. Ikeda, Y. Matsuda, A. Carrington, and T. Shibauchi, *Phys. Rev. B* **82**, 014526 (2010).
- [43] E. Abrahams and Q. Si, *J. Phys. Condens. Matter* **23**, 223201 (2011).
- [44] L. Zhu, M. Garst, A. Rosch, and Q. Si, *Phys. Rev. Lett.* **91**, 066404 (2003).
- [45] M. Garst and A. Rosch, *Phys. Rev. B* **72**, 205129 (2005).
- [46] R. Yu, J.-X. Zhu, and Q. Si, *Curr. Opin. Solid State Mater. Sci.* **17**, 65 (2013).
- [47] L. de' Medici, G. Giovannetti, and M. Capone, *Phys. Rev. Lett.* **112**, 177001 (2014).
- [48] A. Georges, L. d. Medici, and J. Mravlje, *Annu. Rev. Condens. Matter Phys.* **4**, 137 (2013).
- [49] S. Backes, H. O. Jeschke, and R. Valentí, *Phys. Rev. B* **92**, 195128 (2015).
- [50] R. Yu and Q. Si, *Phys. Rev. B* **86**, 085104 (2012).
- [51] J. G. Storey, J. W. Loram, J. R. Cooper, Z. Bukowski, and J. Karpinski, *Phys. Rev. B* **88**, 144502 (2013).
- [52] P. Walmsley, C. Putzke, L. Malone, I. Guillamón, D. Vignolles, C. Proust, S. Badoux, A. I. Coldea, M. D. Watson, S. Kasahara, Y. Mizukami, T. Shibauchi, Y. Matsuda, and A. Carrington, *Phys. Rev. Lett.* **110**, 257002 (2013).
- [53] Y. Nakajima, R. Wang, T. Metz, X. Wang, L. Wang, H. Cynn, S. T. Weir, J. R. Jeffries, and J. Paglione, *Phys. Rev. B* **91**, 060508 (2015).
- [54] A. E. Böhmer, F. Hardy, L. Wang, T. Wolf, P. Schweiss, and C. Meingast, *Nat. Commun.* **6**, 7911 (2015).
- [55] S. Kasahara, T. Shibauchi, K. Hashimoto, K. Ikada, S. Tonegawa, R. Okazaki, H. Shishido, H. Ikeda, H. Takeya, K. Hirata, T. Terashima, and Y. Matsuda, *Phys. Rev. B* **81**, 184519 (2010).
- [56] L. E. Klintberg, S. K. Goh, S. Kasahara, Y. Nakai, K. Ishida, M. Sutherland, T. Shibauchi, Y. Matsuda, and T. Terashima, *J. Phys. Soc. Jpn.* **79**, 123706 (2010).
- [57] P. Monthoux and D. J. Scalapino, *Phys. Rev. Lett.* **72**, 1874 (1994).
- [58] T. Moriya and K. Ueda, *Adv. Phys.* **49**, 555 (2000).

SUPPLEMENTARY MATERIAL –

Strain-driven approach to quantum criticality in $A\text{Fe}_2\text{As}_2$ with $A = \text{K}, \text{Rb}$, and Cs

Felix Eilers,¹ Kai Grube,¹ Diego A. Zocco,¹ Thomas Wolf,¹ Michael Merz,¹ Peter Schweiss,¹ Rolf Heid,¹ Robert Eder,¹ Rong Yu,² Jian-Xin Zhu,³ Qimiao Si,⁴ Takasada Shibauchi,^{5,6} and Hilbert v. Löhneysen^{1,7}

¹*Institut für Festkörperphysik, Karlsruher Institut für Technologie, 76021 Karlsruhe, Germany*

²*Department of Physics, Renmin University of China, Beijing 100872, China*

³*Theoretical Division, Los Alamos National Laboratory, Los Alamos, New Mexico 87545, USA*

⁴*Department of Physics and Astronomy, Rice University, Houston, TX 77005, USA*

⁵*Department of Advanced Materials Science, University of Tokyo, Kashiwa, Chiba 277-8561, Japan*

⁶*Department of Physics, Kyoto University, Sakyo-ku, Kyoto 606-8502, Japan*

⁷*Physikalisch Institut, Karlsruhe Institut für Technologie, 76049 Karlsruhe, Germany*

EXPERIMENTAL DETAILS

Sample growth and crystal structure

Single crystals of KFe_2As , RbFe_2As_2 and CsFe_2As_2 were grown from arsenic-rich flux (composition 0.40 : 0.05 : 0.55 A :Fe:As) in alumina crucibles, as reported in Ref. 11. The crucibles were sealed in an iron tube filled with argon gas. The growth conditions for each of the three compounds have been determined individually to optimize the sample quality. The maximum (minimum) temperatures were 1000 °C (730 °C), 980 °C (690 °C), and 950 °C (800 °C), and cooling rates in the range of 0.3–0.49 °C/h, 0.76 °C/h, and 0.2–0.25 °C/h for $A = \text{K}, \text{Rb}$, and Cs , respectively. Once the lower temperature was reached, the iron tubes were tilted to separate the crystals from the liquid flux, followed by a slow cool-down to room temperature. The small amounts of remaining solid flux residues trapped between the free standing crystals were removed by etching with ethanol.

The crystal structures were examined with four-circle X-ray diffraction at room temperature. Structural refinement confirmed the space group for the three compounds to be $I4/mmm$ and the compositions to be stoichiometric within the error of the experiment (0.5–1%). The lattice parameters were determined to be $a = 3.844(2)$ Å, $c = 13.87(3)$ Å, $z = 0.35241(7)$ for KFe_2As_2 , $a = 3.872(4)$ Å, $c = 14.46(5)$ Å, $z = 0.3475(3)$ for RbFe_2As_2 and $a = 3.902(2)$ Å, $c = 15.14(2)$ Å, $z = 0.3416(4)$ for CsFe_2As_2 . Figure S1 shows the structural parameters of KFe_2As_2 , RbFe_2As_2 and CsFe_2As_2 in comparison with CaFe_2As_2 , SrFe_2As_2 and BaFe_2As_2 . The c parameter increases steadily with the eight-fold coordinated ion radius of the alkaline or alkaline earth atom R_A . The tetrahedron of arsenic atoms surrounding the iron atoms is compressed along the c direction for $AE = \text{Ca}, \text{Sr}, \text{Ba}$ and elongated along c for $A = \text{K}, \text{Rb}, \text{Cs}$. The crystal structure of CsFe_2As_2 is very similar to that of $\text{Ba}_{0.5}\text{K}_{0.5}\text{Fe}_2\text{As}_2$. The iron-iron distance $d_{\text{Fe}-\text{Fe}} = a/\sqrt{2}$ as well as the iron-arsenic distance $d_{\text{Fe}-\text{As}}$ change only little in the $A = \text{K}, \text{Rb}, \text{Cs}$ series.

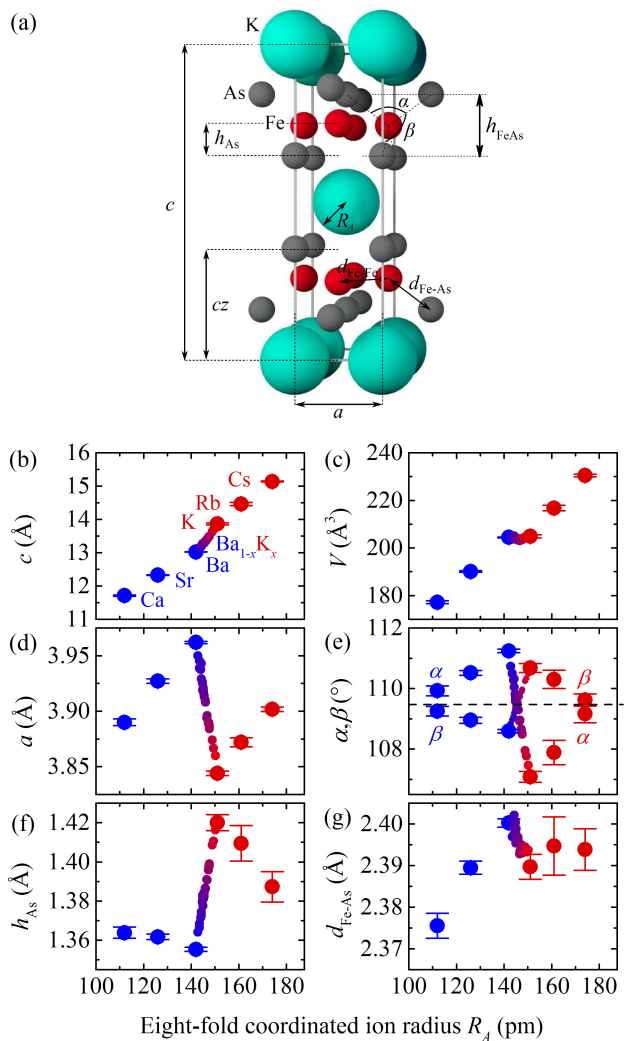


FIG. S1. (Color online) (a) Conventional tetragonal unit cell of $A\text{Fe}_2\text{As}_2$. (b-g) Structural parameters for $A = \text{K}, \text{Rb}, \text{Cs}$ and $AE = \text{Ca}, \text{Sr}, \text{Ba}$ plotted against the eight-fold coordinated anion radius R_A .

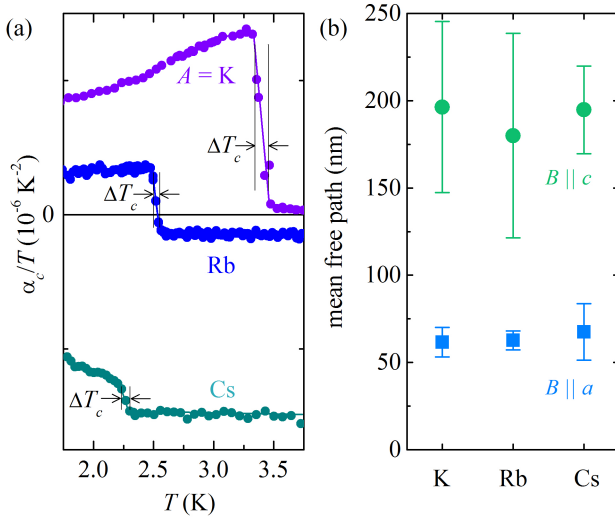


FIG. S2. (a) Linear thermal expansion coefficient along the c axis divided by T of $A\text{Fe}_2\text{As}_2$. (b) The mean free paths l_{mfp} of the studied $A\text{Fe}_2\text{As}_2$ samples with $A = \text{K}, \text{Rb}, \text{Cs}$ extracted from the magnetic field dependence of the observed quantum oscillations for fields parallel and perpendicular to the c axis (see text for details). The lowest and highest values for different samples of each compound are indicated by bars while the filled symbols represent the mean values. The mean free paths do not show significant changes with A . Therefore, the T_c reduction cannot be explained with a degradation of the sample quality.

Thermal expansion

The magnetostriction and thermal expansion have been measured using a parallel-plate capacitance dilatometer operated in a dilution refrigerator, at temperatures between 20 mK and 10 K and at magnetic fields up to 14 T. Changes in length of the crystals were measured both along the c and the a direction for each direction of the applied magnetic field, along c and along a . The superconducting transition temperatures (midpoints) obtained from the thermal expansion measurements at zero magnetic field amount to 3.400 ± 0.047 K, 2.5 ± 0.025 K, and 2.265 ± 0.035 K for $A = \text{K}, \text{Rb}$, and Cs , respectively. The width (10 % - 90 %) of the superconducting transitions of all samples amounts to less than 0.1 K, independently of the alkali-metal ion [see Fig. S2(a)]. The thermal expansion and magnetostriction were measured with a negligible stress (< 1 bar) exerted by the spring suspension of the dilatometer. Hence, the obtained strain dependences reflect initial changes due to infinitesimal uniaxial pressures. Taking into account the tetragonal crystal symmetry, this leads to the equalities: $\partial\gamma/\partial\epsilon_a = \partial\gamma/\partial\epsilon_b$ and $\partial T_c/\partial\epsilon_a = \partial T_c/\partial\epsilon_b$.

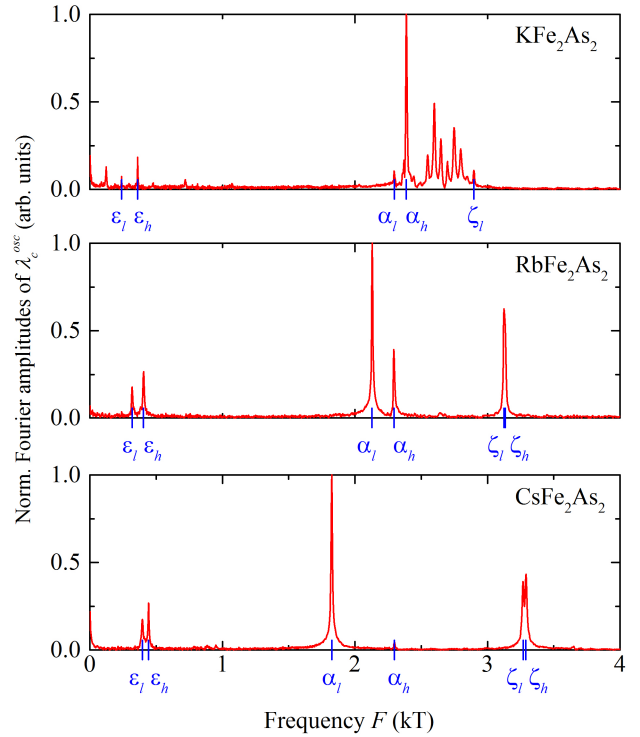


FIG. S3. (Color online) Fourier spectra of the oscillatory part of the magnetostriction coefficient λ_c^{osc} for $B \parallel c$. For clarity only the contribution below $F = 4$ kT along the c axis is shown. The spectra are normalized to the maximum amplitude observed in each spectrum. The fundamental frequencies are labeled by the corresponding Fermi-surface sheets [see inset of Fig. 2(b) of the manuscript].

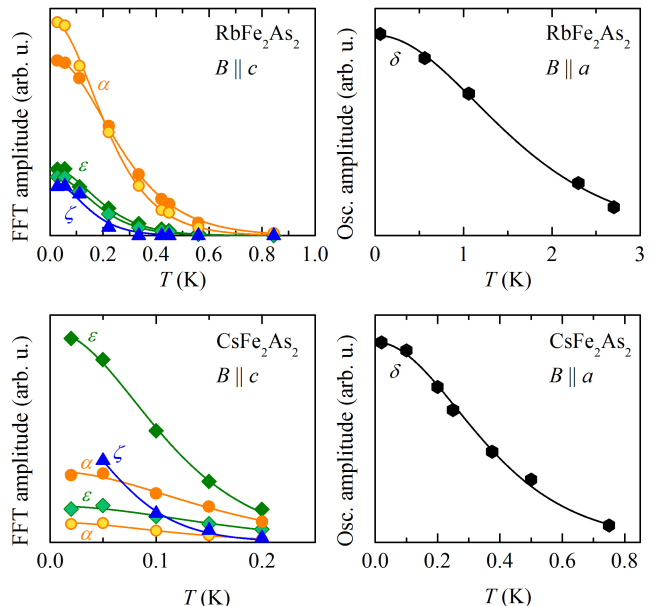


FIG. S4. Fourier amplitudes ($B \parallel c$) and oscillation amplitudes ($B \parallel a$) plotted against temperature. Lines are fits of the temperature factor.

Magnetostriction and quantum oscillations

The magnetostriction was measured at constant temperature by recording the sample length during field sweeps using a rate between 0.02 T/min and 0.1 T/min. Due to eddy-current heating the lowest measuring temperature was limited to 50 mK. To analyze the quantum oscillations observed in the magnetostriction, the derivative of the sample length with respect to the magnetic field was calculated and the oscillatory part was extracted by subtracting a polynomial of low order. The fundamental frequencies were extracted from the Fourier spectra of the oscillatory part of the magnetostriction coefficients $\lambda_i \equiv L_i^{-1} \partial L_i / \partial B$, where L_i is the length of the crystal in the $i = a, c$ direction and $B = \mu_0 H$ is the applied magnetic field.

We determined the mean free path l_{mfp} of our samples by analyzing the field dependent amplitudes of the α_l and α_h frequencies for $B \parallel c$ and of δ for $B \perp c$ at constant temperature using the Dingle factor in the Lifshitz-Kosevich formula [13, 42]. The l_{mfp} values are shown in Fig. S2. The spread of the values is indicated by the vertical bars while the mean values are represented by filled symbols, circles and squares for B parallel and perpendicular to the c axis, respectively. The relative error for determining l_{mfp} for individual samples is less than ± 5 nm. Due to the layered structure of the crystals l_{mfp} is larger in the ab plane than in c direction. With increasing R_A no significant change of l_{mfp} can be observed. Moreover, independently of the slightly differing l_{mfp} , all samples of the same compound show identical T_c values within our experimental error of less than 0.02 K and similar T_c widths. In conclusion, our samples do not exhibit significant quality changes.

Figure S3 shows a magnified view of the Fourier spectra normalized to the maximum amplitude of each spectrum at frequencies below 4 kT. For clarity we only show the λ_c spectra for $B \parallel c$. The amplitudes reflect the uniaxial pressure dependence of the related extremal Fermi-surface orbits. The amplitude of the α_h orbit exhibits a strong reduction compared to that of α_l . This might be due to the weak chemical pressure dependence of α_l , which might also explain the failure to observe the magnetostriction oscillations of the β -band [see Fig. 2(a) of the manuscript].

Values of the effective quasiparticle mass m^* have been inferred from the temperature dependence of the quantum oscillations by using the Lifshitz-Kosevich formula [12, 13]. Figure S4 displays the fits for the Fermi-surface sheets obtained for $B \parallel a$ and c .

THEORETICAL CALCULATIONS

Elastic constants

To obtain rough estimates of the elastic constants we performed ab-initio calculations of electronic and vibrational properties of $A\text{Fe}_2\text{As}_2$ ($A = \text{K}, \text{Rb}, \text{Cs}$) in the framework of the generalized gradient approximation using a mixed-basis pseudopotential method [43]. Phonon dispersions and corresponding interatomic force constants were calculated via density functional perturbation theory [44]. The elastic constants were then derived via the method of long waves, which relates the elastic constants to sums over force constants weighted by the bond vector [45]. All calculations used experimental lattice structures, and employed normconserving pseudopotentials with a plane-wave cutoff of 22 Ry, augmented by local functions at the sites of both Fe and the alkaline metals. Brillouin zone summations were done with a Gaussian broadening technique using a broadening of 0.1 eV and 40 wave vector points in the irreducible part of the Brillouin zone. Additional technical details can be found in Ref. [46, 47], where the same approach has been applied to studies of the vibrational properties of CaFe_2As_2 and BaFe_2As_2 . We obtain the following sets of elastic constants c_{ij} with $i, j = 1 \dots 3$ and bulk moduli B_T for KFe_2As_2 (in GPa):

$$c_{ij} = \begin{pmatrix} 79.7 & 46.6 & 38.4 \\ & 79.7 & 38.4 \\ & & 45.1 \end{pmatrix}, B_T = 43.7 \text{ GPa}, \quad (1)$$

for RbFe_2As_2 (in GPa):

$$c_{ij} = \begin{pmatrix} 78.3 & 40.2 & 28.4 \\ & 78.3 & 28.4 \\ & & 53.8 \end{pmatrix}, B_T = 42.3 \text{ GPa}, \quad (2)$$

and for CsFe_2As_2 (in GPa):

$$c_{ij} = \begin{pmatrix} 84.4 & 45.9 & 39.5 \\ & 84.4 & 39.5 \\ & & 61.2 \end{pmatrix}, B_T = 51.3 \text{ GPa}. \quad (3)$$

The measured bulk modulus of KFe_2As_2 amounts to 40 ± 1 GPa [17].

Electron correlations

To consider the correlation effects in theory, we study a multiorbital Hubbard model for the $A\text{Fe}_2\text{As}_2$ ($A = \text{K}, \text{Rb}, \text{Cs}$) system. The Hamiltonian reads

$$H = H_0 + H_{\text{int}}. \quad (4)$$

H_0 contains the tight-binding parameters among the multiple orbitals of $A\text{Fe}_2\text{As}_2$.

$$H_0 = \frac{1}{2} \sum_{ij\alpha\beta\sigma} t_{ij}^{\alpha\beta} d_{i\alpha\sigma}^\dagger d_{j\beta\sigma} + \sum_{i\alpha\sigma} (\Delta_\alpha - \mu) d_{i\alpha\sigma}^\dagger d_{i\alpha\sigma}, \quad (5)$$

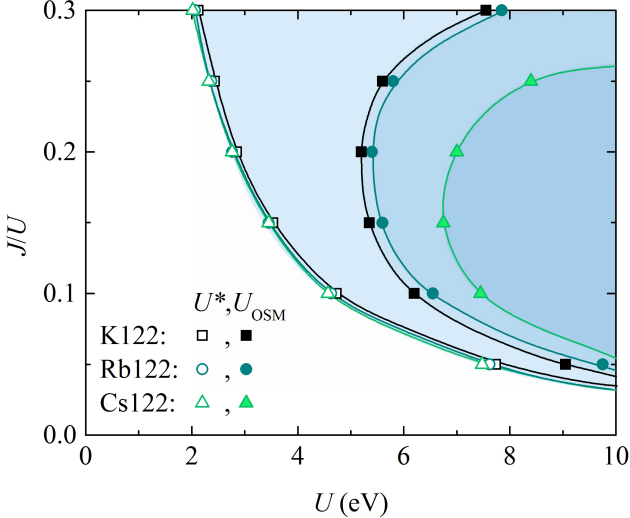


FIG. S5. (Color online) Ground-state phase diagram of KFe_2As_2 , RbFe_2As_2 , and CsFe_2As_2 in the J/U - U plane from slave-spin mean-field theory. The open and closed symbols show the crossover at U^* , and the critical U value for the orbital-selective Mott transition, U_{OSM} , respectively.

where $d_{i\alpha\sigma}^\dagger$ creates an electron in orbital α with spin σ at site i , Δ_α is the on-site energy reflecting the crystal field splitting, and μ is the chemical potential. The details of the tight-binding parameters will be discussed in the next section of this Supplementary Material. H_{int} contains on-site Hubbard interactions

$$H_{\text{int}} = \frac{U}{2} \sum_{i,\alpha,\sigma} n_{i\alpha\sigma} n_{i\alpha\bar{\sigma}} + \sum_{i,\alpha<\beta,\sigma} \{ U' n_{i\alpha\sigma} n_{i\beta\bar{\sigma}} + (U' - J) n_{i\alpha\sigma} n_{i\beta\sigma} - J(d_{i\alpha\sigma}^\dagger d_{i\alpha\bar{\sigma}} d_{i\beta\bar{\sigma}}^\dagger d_{i\beta\sigma} - d_{i\alpha\sigma}^\dagger d_{i\alpha\bar{\sigma}}^\dagger d_{i\beta\sigma} d_{i\beta\bar{\sigma}}) \} \quad (6)$$

where $n_{i\alpha\sigma} = d_{i\alpha\sigma}^\dagger d_{i\alpha\sigma}$. In this model, U , U' , and J respectively denote the intraorbital repulsion, the interorbital repulsion, and the Hund's rule exchange coupling. We take $U' = U - 2J$ as is standard [48].

We study the model via a U(1) slave-spin approach [38]. Within this theory, the effect of electron correlations can be characterized by the orbital-resolved quasiparticle spectral weight, Z_α , which we will calculate in the paramagnetic phase at the electron filling of $n = 5.5$ electrons per Fe ion. The results are summarized in the ground-state phase diagram given in Fig. S5. Because N is not an integer, no metal-to-insulator transition is observed; the system is always metallic for any U and J values. We do however find, for a fixed J and with increasing U , a crossover at U^* from a weakly correlated regime (with $Z_\alpha \sim 1$) to a regime with strong correlation ($Z_\alpha \ll 1$). Further increasing U (or J for a fixed U) drives the system into an orbital-selective Mott

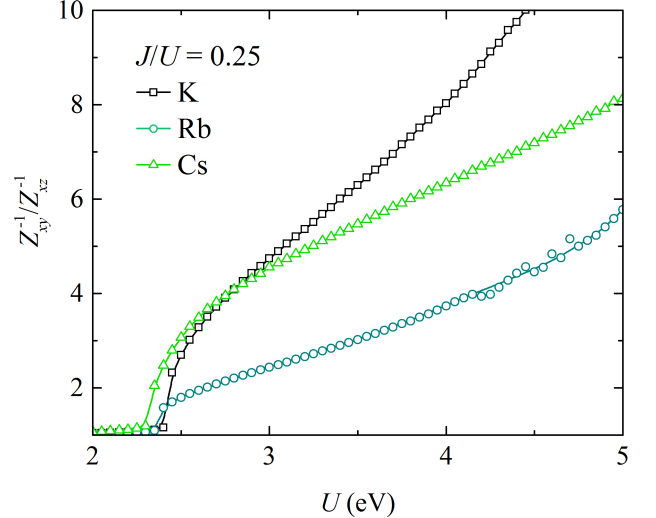


FIG. S6. (Color online) Evolution of the ratio Z_{xy}^{-1}/Z_{xz}^{-1} with U at $J/U = 0.25$ in the models for KFe_2As_2 , RbFe_2As_2 , and CsFe_2As_2 . Z_{xy}^{-1}/Z_{xz}^{-1} is proportional to the ratio of mass enhancement of d_{xy} orbital to d_{xz} orbital. For $U \gtrsim 2.5$ eV, a wide regime with strong orbital selectivity exists for the three compounds, with the heaviest orbital to be the $3d_{xy}$.

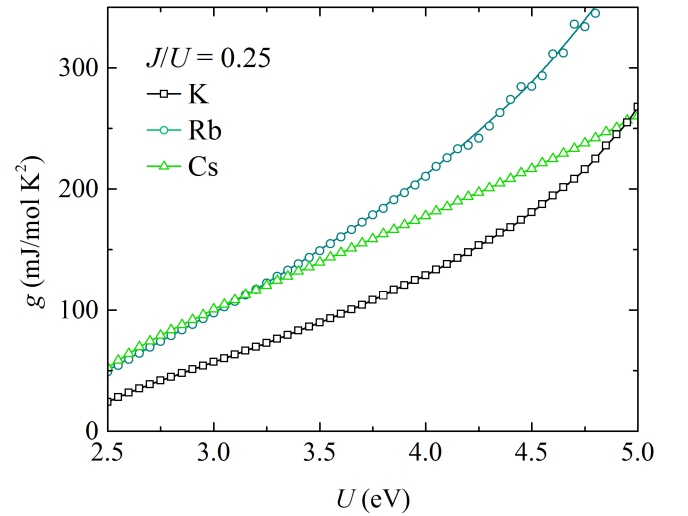


FIG. S7. (Color online) The evolution of g with U . The definition of g is given in Eq. 7. g behaves in a similar way to γ in the regime with strong electron correlations.

phase (OSMP) in which the $3d_{xy}$ orbital of Fe is Mott localized (with $Z_{xy} = 0$) while the other $3d$ orbitals are still itinerant (with $Z > 0$). We find that the critical value of the orbital-selective Mott transition (OSMT), U_{OSM} , shows strong material dependence from K to Cs, and in general $U_{OSM} \gtrsim 5.5$ eV, while U^* is comparable for all the three compounds, and can be as low as ~ 2.3 eV for $J/U = 0.25$. Therefore, there is a large regime in the phase diagram that shows strong orbital selectivity, as demonstrated in Fig. S6. It is also an interesting obser-

vation that similar strong orbital selectivity shown in the phase diagram for these heavily hole doped iron pnictides also exists in the phase diagrams for some parent and electron doped iron pnictides and iron selenides [38, 49].

The effect of strong electron correlations is also manifested through the Sommerfeld coefficient γ . We have calculated γ by taking the second derivative of the free energy with respect to temperature, namely, $\gamma = -\partial^2 f / \partial T^2$. The results for the three compounds are shown in Fig. 3(b) of the main text. We find that for each of the three compounds, γ is enhanced in the regime of phase diagram that exhibits strong electron correlations. Remarkably, within a certain range of U and J (2.5 eV $\lesssim U \lesssim 5$ eV for $J/U = 0.25$, for example), the calculated values of γ are about $100 \sim 200$ mJ/mol K 2 , which are of the same order as the experimental values for these compounds.

In the slave-spin approach, an analytical expression of γ is difficult to obtain due to the multiorbital nature. However, we can gain insights into the behavior of γ from an approximate quantity, g . In the regime of phase diagram showing strong orbital selectivity, the inter-orbital correlations are suppressed by the combined effects of Hund's coupling and crystal level splitting. Therefore, to a good approximation, each orbital contributes to γ independently. We therefore define

$$g = \sum_{\alpha} \mathfrak{N}_{\alpha}(E_F)/Z_{\alpha}, \quad (7)$$

where $\mathfrak{N}_{\alpha}(E_F)$ is the electron density of states at the Fermi energy projected onto orbital α in the noninteracting limit. Fig. S7 shows the evolution of g with U , calculated with the same model parameters as in Fig. 3(b) of the main text. The qualitatively similar behavior of

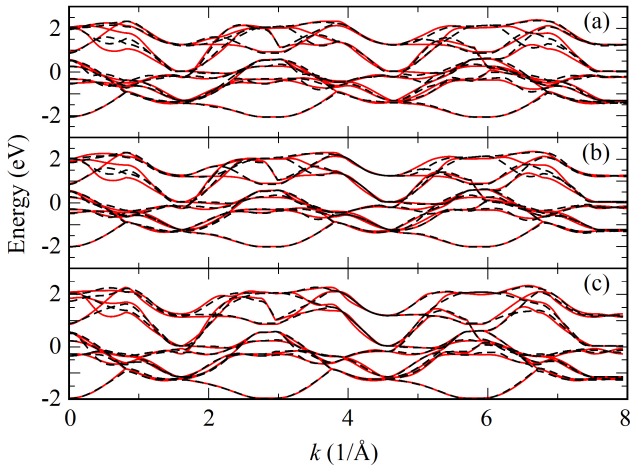


FIG. S8. (Color online) The five-orbital tight-binding fit (dashed black lines) of the 10 Wannier fit (solid red lines) for KFe₂As₂ (a), RbFe₂As₂ (b), CsFe₂As₂ (c). All energies are measured with respect to the Fermi energy. The wave vector k -path is chosen to be along the high symmetry points.

g and γ implies the same underlying physics. From the definition of g , we see that the enhancement of g (and γ) originates from the mass enhancement of each orbital, which is proportional to $1/Z_{\alpha}$. Due to the strong orbital selectivity (Fig. S6), the $3d_{xy}$ orbital is the heaviest, and contributes to g (and γ) the most. At the OSMT, the d_{xy} orbital is fully decoupled from other orbitals, and $Z_{xy} = 0$. As a consequence, g and γ diverge as the OSMT is approached. This provides one way to understand the strongly enhanced γ .

However, for a fixed set of U and J values, γ does not increase monotonically from K to Cs. As discussed in the main text, this implicates an additional contribution to γ associated with AF quantum criticality. A natural candidate is a quantum critical point (QCP) for an AF ordering associated with the Mott insulating state at $N = 5$; the latter has been advanced in Ref. 34 and illustrated in Fig. 4 of the main text.

DFT calculations and tight-binding parameters

We have performed band-structure calculations for KFe₂As₂, RbFe₂As₂ and CsFe₂As₂ based on the generalized gradient approximation. Within the limitation of the calculations and the experimental errors, the calculated band structure agrees with recent angle-resolved photoemission spectroscopy measurements [4, 50, 51]. The full-potential linearized augmented plane wave (FP-LAPW) method as implemented in the WIEN2K code [52] is used. We then follow the procedure suggested by Graser *et al.* [53] to fit the Wannierized bands [54, 55] with a five-orbital tight-binding Hamiltonian [56], by unfolding the Brillouin zone with two Fe sites per unit cell to the Brillouin zone corresponding to one Fe site per unit cell. In this procedure, an interface [57] between the WIEN2k code and the wannier90 code [58] has also been employed to disentangle the bands. We show in Fig. S8 the comparison of the tight-binding fit to those obtained from the GGA-based Wannier orbitals for the three 122 compounds. The corresponding tight-binding model parameters are listed in Tables S1-S3.

	$\alpha = 1$	$\alpha = 2$	$\alpha = 3$	$\alpha = 4$	$\alpha = 5$						
ϵ_α	0.27530	0.27530	-0.37164	0.69843	0.1381						
$t_\mu^{\alpha\alpha}$	$\mu = x$	$\mu = y$	$\mu = xy$	$\mu = xx$	$\mu = xxy$	$\mu = yy$	$\mu = xyy$	$\mu = xxyy$	$\mu = z$	$\mu = xz$	$\mu = xxz$
$\alpha = 1$	-0.08418	-0.19954	0.06963	0.24664	-0.07912	0.03223	0.01942			-0.00580	0.04127
$\alpha = 3$	0.36702		0.02663	-0.08301							
$\alpha = 4$	0.15386		-0.05682	0.10419	-0.01544		-0.06894	0.09484	0.06175		0.02122
$\alpha = 5$	-0.02496		-0.12021		-0.01013		0.02655	0.03076	-0.02373		
$t_\mu^{\alpha\beta}$	$\mu = x$	$\mu = xy$	$\mu = xxy$	$\mu = xyy$	$\mu = z$	$\mu = xz$	$\mu = xyz$	$\mu = xxyz$			
$\alpha\beta = 12$		-0.14893	-0.06209	-0.03947			0.01886				
$\alpha\beta = 13$	-0.43065	-0.00736	-0.05048								
$\alpha\beta = 14$	0.21335	-0.06953	0.05399			-0.00344	0.00223	-0.00263			
$\alpha\beta = 15$	-0.19991	-0.14116		0.00000			-0.00153				
$\alpha\beta = 24$					0.03195			0.01817			
$\alpha\beta = 34$			-0.05942								
$\alpha\beta = 35$	-0.22330		0.05165								
$\alpha\beta = 45$		-0.30785		0.00160	-0.08049	0.01885					

Table S1. Tight-binding parameters of the five-orbital model for KFe₂As₂. Here we use the same notation as in Ref. 53. The orbital indeces $\alpha = 1, 2, 3, 4, 5$ correspond to d_{xz} , d_{yz} , $d_{x^2-y^2}$, d_{xy} , and $d_{3z^2-r^2}$ orbitals, respectively. The units of the parameters are eV.

	$\alpha = 1$	$\alpha = 2$	$\alpha = 3$	$\alpha = 4$	$\alpha = 5$						
ϵ_α	0.32345	0.32345	-0.40194	0.71731	0.14450						
$t_\mu^{\alpha\alpha}$	$\mu = x$	$\mu = y$	$\mu = xy$	$\mu = xx$	$\mu = xxy$	$\mu = yy$	$\mu = xyy$	$\mu = xxyy$	$\mu = z$	$\mu = xz$	$\mu = xxz$
$\alpha = 1$	-0.06985	-0.22598	0.08377	0.24043	-0.06168	0.02105	0.01175			-0.00650	0.03774
$\alpha = 3$	0.35885		0.05108	-0.09566							
$\alpha = 4$	0.13022		-0.07484	0.10261	-0.00952		-0.05511	0.09126	0.05656		0.01980
$\alpha = 5$	-0.02614		-0.12488		-0.00458		0.03092	0.02191	-0.01853		
$t_\mu^{\alpha\beta}$	$\mu = x$	$\mu = xy$	$\mu = xxy$	$\mu = xyy$	$\mu = z$	$\mu = xz$	$\mu = xyz$	$\mu = xxyz$			
$\alpha\beta = 12$		-0.18759	-0.05309	-0.03053			0.01131				
$\alpha\beta = 13$	-0.29129	-0.03934	-0.00812								
$\alpha\beta = 14$	0.16066	-0.10845	0.06566			0.00170	0.00105	-0.00054			
$\alpha\beta = 15$	-0.16746	-0.15103		-0.00000			-0.01179				
$\alpha\beta = 24$					0.02094			0.02331			
$\alpha\beta = 34$			-0.03127								
$\alpha\beta = 35$	-0.35706		-0.02342								
$\alpha\beta = 45$		-0.31169		0.00551	-0.06925	0.01886					

Table S2. Tight-binding parameters of the five-orbital model for RbFe₂As₂. Here we use the same notation as in Ref. 53. The orbital index $\alpha = 1, 2, 3, 4, 5$ correspond to d_{xz} , d_{yz} , $d_{x^2-y^2}$, d_{xy} , and $d_{3z^2-r^2}$ orbitals, respectively. The units of the parameters are eV.

	$\alpha = 1$	$\alpha = 2$	$\alpha = 3$	$\alpha = 4$	$\alpha = 5$						
ϵ_α	0.28734	0.28734	-0.16395	0.62596	0.15918						
$t_\mu^{\alpha\alpha}$	$\mu = x$	$\mu = y$	$\mu = xy$	$\mu = xx$	$\mu = xxy$	$\mu = yy$	$\mu = xyy$	$\mu = xxyy$	$\mu = z$	$\mu = xz$	$\mu = xxz$
$\alpha = 1$	-0.11178	-0.27610	0.06091	0.23489	-0.02882	0.03720	0.02428			-0.00318	0.00724
$\alpha = 3$	0.35911		-0.00843	-0.08560							
$\alpha = 4$	0.09760		-0.02986	0.09725	0.00281		-0.07308	0.09810	0.04760		0.01886
$\alpha = 5$	-0.04504		-0.11908		0.01105		0.03144	0.02875	-0.01499		
$t_\mu^{\alpha\beta}$	$\mu = x$	$\mu = xy$	$\mu = xxy$	$\mu = xyy$	$\mu = z$	$\mu = xz$	$\mu = xyz$	$\mu = xxyz$			
$\alpha\beta = 12$		-0.09741	-0.01353	-0.03424			-0.02276				
$\alpha\beta = 13$	-0.45003	0.05198	-0.03004								
$\alpha\beta = 14$	0.25147	-0.05763	0.04722			-0.00347	-0.00706	-0.00007			
$\alpha\beta = 15$	-0.23510	-0.10405		-0.00000			0.00193				
$\alpha\beta = 24$					0.01628			0.01794			
$\alpha\beta = 34$		-0.04939									
$\alpha\beta = 35$	-0.23635		0.03186								
$\alpha\beta = 45$		-0.27431		-0.00219	0.01117	0.02361					

Table S3. Tight-binding parameters of the five-orbital model for CsFe₂As₂. Here we use the same notation as in Ref. 53. The orbital index $\alpha = 1, 2, 3, 4, 5$ correspond to d_{xz} , d_{yz} , $d_{x^2-y^2}$, d_{xy} , and $d_{3z^2-r^2}$ orbitals, respectively. The units of the parameters are eV.

-
- [1] T. Shibauchi, A. Carrington, and Y. Matsuda, Annual Review of Condensed Matter Physics **5**, 113 (2014).
- [2] J. Dai, Q. Si, J.-X. Zhu, and E. Abrahams, PNAS **106**, 4118 (2009).
- [3] Y. G. Naidyuk, O. E. Kvintitskaya, N. V. Gamayunova, L. Boeri, S. Aswartham, S. Wurmehl, B. Büchner, D. V. Efremov, G. Fuchs, and S.-L. Drechsler, Phys. Rev. B **90**, 094505 (2014).
- [4] K. Okazaki, Y. Ota, Y. Kotani, W. Malaeb, Y. Ishida, T. Shimojima, T. Kiss, S. Watanabe, C.-T. Chen, K. Kihou, C. H. Lee, A. Iyo, H. Eisaki, T. Saito, H. Fukazawa, Y. Kohori, K. Hashimoto, T. Shibauchi, Y. Matsuda, H. Ikeda, H. Miyahara, R. Arita, A. Chainani, and S. Shin, Science **337**, 1314 (2012).
- [5] J.-P. Reid, M. A. Tanatar, A. Juneau-Fecteau, R. T. Gordon, S. R. de Cotret, N. Doiron-Leyraud, T. Saito, H. Fukazawa, Y. Kohori, K. Kihou, C. H. Lee, A. Iyo, H. Eisaki, R. Prozorov, and L. Taillefer, Phys. Rev. Lett. **109**, 087001 (2012).
- [6] X. C. Hong, X. L. Li, B. Y. Pan, L. P. He, A. F. Wang, X. G. Luo, X. H. Chen, and S. Y. Li, Phys. Rev. B **87**, 144502 (2013).
- [7] Z. Zhang, A. F. Wang, X. C. Hong, J. Zhang, B. Y. Pan, J. Pan, Y. Xu, X. G. Luo, X. H. Chen, and S. Y. Li, Phys. Rev. B **91**, 024502 (2015).
- [8] F. Hardy, A. E. Böhmer, D. Aoki, P. Burger, T. Wolf, P. Schweiss, R. Heid, P. Adelmann, Y. X. Yao, G. Kotliar, J. Schmalian, and C. Meingast, Phys. Rev. Lett. **111**, 027002 (2013).
- [9] A. F. Wang, B. Y. Pan, X. G. Luo, F. Chen, Y. J. Yan, J. J. Ying, G. J. Ye, P. Cheng, X. C. Hong, S. Y. Li, and X. H. Chen, Phys. Rev. B **87**, 214509 (2013).
- [10] T. Terashima, N. Kurita, M. Kimata, M. Tomita, S. Tsuchiya, M. Imai, A. Sato, K. Kihou, C.-H. Lee, H. Kito, H. Eisaki, A. Iyo, T. Saito, H. Fukazawa, Y. Ko-

- hori, H. Harima, and S. Uji, Phys. Rev. B **87**, 224512 (2013).
- [11] D. A. Zocco, K. Grube, F. Eilers, T. Wolf, and H. v. Löhneysen, Phys. Rev. Lett. **111**, 057007 (2013).
- [12] D. A. Zocco, K. Grube, F. Eilers, T. Wolf, and H. v. Löhneysen, JPS Conf. Proc. **3**, 015007 (2014).
- [13] D. Shoenberg, *Magnetic oscillations in metals* (Cambridge University Press, 1984).
- [14] V. Taufour, N. Foroozani, M. A. Tanatar, J. Lim, U. Kaluarachchi, S. K. Kim, Y. Liu, T. A. Lograsso, V. G. Kogan, R. Prozorov, S. L. Bud'ko, J. S. Schilling, and P. C. Canfield, Phys. Rev. B **89**, 220509 (2014).
- [15] L.-Y. T. Jian-Jun Ying and, V. V. Struzhkin, H.-K. Mao, A. G. Gavriliiuk, A.-F. Wang, X.-H. Chen, and X.-J. Chen, arXiv:1501.00330 (2015).
- [16] P. Burger, F. Hardy, D. Aoki, A. E. Böhmer, R. Eder, R. Heid, T. Wolf, P. Schweiss, R. Fromknecht, M. J. Jackson, C. Paulsen, and C. Meingast, Phys. Rev. B **88**, 014517 (2013).
- [17] F. F. Tafti, J. P. Clancy, M. Lapointe-Major, C. Collignon, S. Faucher, J. A. Sears, A. Juneau-Fecteau, N. Doiron-Leyraud, A. F. Wang, X.-G. Luo, X. H. Chen, S. Desgreniers, Y.-J. Kim, and L. Taillefer, Phys. Rev. B **89**, 134502 (2014).
- [18] J. Kanter, Z. Bukowski, J. Karpinski, and B. Batlogg, “Heavy quasi particle mass in (Rb,Cs)Fe₂As₂,” in *Annual Report of the Laboratory for Solid State Physics* (ETH Zürich, Department of Physics, 2010).
- [19] S. Drotziger, P. Schweiss, K. Grube, T. Wolf, P. Adelmann, C. Meingast, and H. v. Lhneysen, Journal of the Physical Society of Japan **79**, 124705 (2010).
- [20] E. Granado, L. Mendonça Ferreira, F. Garcia, G. d. M. Azevedo, G. Fabbris, E. M. Bittar, C. Adriano, T. M. Garitezi, P. F. S. Rosa, L. F. Bufaiçal, M. A. Avila, H. Terashita, and P. G. Pagliuso, Phys. Rev. B **83**, 184508 (2011).

- [21] Z. P. Yin, K. Haule, and G. Kotliar, *Nature Materials* **10**, 932 (2011).
- [22] T. T. Ong and P. Coleman, *Phys. Rev. Lett.* **108**, 107201 (2012).
- [23] P. F. S. Rosa, T. M. Adriano, C. Garitezi, T. Grant, Z. Fisk, R. R. Urbano, and P. G. Pagliuso, *Scientific Reports* **4**, 6543 (2014).
- [24] K. Hashimoto, A. Serafin, S. Tonegawa, R. Katsumata, R. Okazaki, T. Saito, H. Fukazawa, Y. Kohori, K. Kihou, C. H. Lee, A. Iyo, H. Eisaki, H. Ikeda, Y. Matsuda, A. Carrington, and T. Shibauchi, *Phys. Rev. B* **82**, 014526 (2010).
- [25] E. Abrahams and Q. Si, *Journal of Physics: Condensed Matter* **23**, 223201 (2011).
- [26] L. Zhu, M. Garst, A. Rosch, and Q. Si, *Phys. Rev. Lett.* **91**, 066404 (2003).
- [27] M. Garst and A. Rosch, *Phys. Rev. B* **72**, 205129 (2005).
- [28] Y. Nakajima, R. Wang, T. Metz, X. Wang, L. Wang, H. Cynn, S. T. Weir, J. R. Jeffries, and J. Paglione, *Phys. Rev. B* **91**, 060508 (2015).
- [29] J. G. Storey, J. W. Loram, J. R. Cooper, Z. Bukowski, and J. Karpinski, *Phys. Rev. B* **88**, 144502 (2013).
- [30] A. E. Böhmer, F. Hardy, L. Wang, T. Wolf, P. Schweiss, and C. Meingast, *Nature Communications* **6**, 7911 (2015).
- [31] P. Walmsley, C. Putzke, L. Malone, I. Guillamón, D. Vignolles, C. Proust, S. Badoux, A. I. Coldea, M. D. Watson, S. Kasahara, Y. Mizukami, T. Shibauchi, Y. Matsuda, and A. Carrington, *Phys. Rev. Lett.* **110**, 257002 (2013).
- [32] S. Kasahara, T. Shibauchi, K. Hashimoto, K. Ikada, S. Tonegawa, R. Okazaki, H. Shishido, H. Ikeda, H. Takeya, K. Hirata, T. Terashima, and Y. Matsuda, *Phys. Rev. B* **81**, 184519 (2010).
- [33] L. E. Klintberg, S. K. Goh, S. Kasahara, Y. Nakai, K. Ishida, M. Sutherland, T. Shibauchi, Y. Matsuda, and T. Terashima, *Journal of the Physical Society of Japan* **79**, 123706 (2010).
- [34] R. Yu, J.-X. Zhu, and Q. Si, *Current Opinion in Solid State and Materials Science* **17**, 65 (2013).
- [35] L. de' Medici, G. Giovannetti, and M. Capone, *Phys. Rev. Lett.* **112**, 177001 (2014).
- [36] A. Georges, L. d. Medici, and J. Mravlje, *Annu. Rev. Condens. Matter Phys.* **4**, 137 (2013).
- [37] S. Backes, H. O. Jeschke, and R. Valentí, *Phys. Rev. B* **92**, 195128 (2015).
- [38] R. Yu and Q. Si, *Phys. Rev. B* **86**, 085104 (2012).
- [39] P. Monthoux and D. J. Scalapino, *Phys. Rev. Lett.* **72**, 1874 (1994).
- [40] T. Moriya and K. Ueda, *Advances in Physics* **49**, 555 (2000).
- [41] See Supplemental Material [*url*], which includes Refs. [42–58].
- [42] E. Fawcett *et al.*, *Electrons at the Fermi surface*, edited by M. Springford (Cambridge University Press, 1980).
- [43] B. Meyer, C. Elsässer, M. Lechermann, and F. Fähnle, *FORTRAN90, a program for mixed-basis pseudopotential calculations for crystals* (MPI für Metallforschung, Stuttgart).
- [44] R. Heid and K.-P. Bohnen, *Phys. Rev. B* **60**, R3709 (1999).
- [45] M. Born and K. Huang, *Dynamical Theory of Crystal Lattices* (Oxford University Press, Oxford, 1954).
- [46] R. Mittal, L. Pintschovius, D. Lamago, R. Heid, K.-P. Bohnen, D. Reznik, S. L. Chaplot, Y. Su, N. Kumar, S. K. Dhar, A. Thamizhavel, and T. Brueckel, *Phys. Rev. Lett.* **102**, 217001 (2009).
- [47] D. Reznik, K. Lokshin, D. C. Mitchell, D. Parshall, W. Dmowski, D. Lamago, R. Heid, K.-P. Bohnen, A. S. Sefat, M. A. McGuire, B. C. Sales, D. G. Mandrus, A. Subedi, D. J. Singh, A. Alatas, M. H. Upton, A. H. Said, A. Cunsolo, Y. Shvyd'ko, and T. Egami, *Phys. Rev. B* **80**, 214534 (2009).
- [48] C. Castellani, C. R. Natoli, and J. Ranninger, *Phys. Rev. B* **18**, 4945 (1978).
- [49] R. Yu and Q. Si, *Phys. Rev. Lett.* **110**, 146402 (2013).
- [50] T. Yoshida, S.-i. Ideta, I. Nishi, A. Fujimori, M. Yi, R. Moore, S.-K. Mo, D. Lu, Z.-X. Shen, Z. Hussain, K. Kihou, C. H. Lee, A. Iyo, H. Eisaki, and H. Harima, *Front. Physics* **2**, 17 (2014).
- [51] S. Kong, D. Y. Liu, S. T. Cui, S. L. Ju, A. F. Wang, X. G. Luo, L. J. Zou, X. H. Chen, G. B. Zhang, and Z. Sun, *Phys. Rev. B* **92**, 184512 (2015).
- [52] P. Blaha, K. Schwarz, G. Madsen, D. Kvasnicka, and J. Luitz, *WIEN2k, An Augmented Plane Wave + Local Orbitals Program for Calculating Crystal Properties* (Karlheinz Schwarz, Techn. Universität Wien, Austria), 2001. ISBN 3-9501031-1-2.
- [53] S. Graser, A. F. Kemper, T. A. Maier, H.-P. Cheng, P. J. Hirschfeld, and D. J. Scalapino, *Phys. Rev. B* **81**, 214503 (2010).
- [54] N. Marzari and D. Vanderbilt, *Phys. Rev. B* **56**, 12847 (1997).
- [55] I. Souza, N. Marzari, and D. Vanderbilt, *Phys. Rev. B* **65**, 035109 (2001).
- [56] S. Graser, T. A. Maier, P. J. Hirschfeld, and D. J. Scalapino, *New Journal of Physics* **11**, 025016 (2009).
- [57] J. Kuneš, R. Arita, P. Wissgott, A. Toschi, H. Ikeda, and K. Held, *Computer Physics Communications* **181**, 1888 (2010).
- [58] A. A. Mostofi, J. R. Yates, Y.-S. Lee, I. Souza, D. Vanderbilt, N. Marzari, A. A. Mostofi, J. R. Yates, Y.-S. Lee, I. Souza, D. Vanderbilt, and N. Marzari, *Computer Physics Communications* **178**, 685 (2008).